PAPER No. DY-11

LAPLACE-DOMAIN SOLUTION OF THE AEROELASTIC PROBLEM OF A ROTOR BLADE IN FORWARD FLIGHT

Fred Nitzsche
Institute for Aerospace Research
National Research Council of Canada
1500, Montreal Road, Building U66A
Ottawa, Ontario, K1A-0R6, Canada

A general continuous frequency domain approach to approximate the time-varying characteristics of a rotor blade in forward flight is presented. The method is particularly useful to obtain a time-invariant equivalent form of the periodic aeroelastic system that allows well-known techniques employed in fixed wings to be extended to rotary wings. The method is first validated solving Mathieu's equation. Next, the two-degree-of-freedom problem of a rotating beam in forward flight is solved in the Laplace domain. The transfer functions between a distributed pressure perturbation applied along the blade and local degrees of freedom are obtained, simulating the effects of parallel blade-vortex-interaction.

NOMENCLATURE

a	distance between the midchord and the pitch axis normalized by the semichord (positive aft)
B_l	boundary condition matrix operator
b	blade semichord
$C(s)$	local lift deficiency function
D	matrix of compliance coefficients
d_{ij}	blade structure compliance coefficients
EI_{ref}	reference bending stiffness
I	unit matrix
I_b	blade mass moment of inertia about the root in the flap direction
J	integrating matrix operator
M	mass matrix
m	mass per unit of length
N	approximation order
n	number of stations along the blade
Q	matrix of aerodynamic influence coefficients
R	rotor radius
r	local radius
r_θ	cross-section radius of gyration about the elastic axis
$s, \bar{s}$	Laplace variable, s/Ω
T	cross section tension
U	airflow local velocity
V	rotor free stream velocity
x	state vector
Z	geometric stiffness matrix

Greek

γ	Lock number
θ	cross-section torsion angle
μ	rotor advance ratio ($V/\Omega R$)
ν	rotational parameter
ρ	air density
φ	cross-section flatwise bending slope
ψ	azimuth angle
Ω	rotor spinning frequency

Superscripts

C	circulatory aerodynamic component
Q	quasisteady aerodynamic component
$\overline{}$	non-dimensional quantity
$\cdot$	derivative with respect to the azimuth angle
$\grave{}$	diagonal matrix built with the elements of a vector

1. INTRODUCTION

When developing individual blade control (IBC) techniques to attenuate rotor noise and vibration, it is desirable to design the control algorithms in the Laplace domain. This ensures that the actuation is not restricted to a harmonic function of the rotor frequency. In addition, it enables the use of previously unavailable well-developed feedback optimal control methods, such as the Linear Quadratic Gaussian, which require time-invariant systems. In this paper, the Laplace domain solution of the

aeroelastic equations of a rotor blade in forward flight, undergoing coupled motion involving both flatwise bending and torsion, is developed. The equations are linearized about an equilibrium position and integrated in space, resulting in a system of differential equations in the time-related independent variable (blade azimuth angle). The transformation of these equations into the Laplace domain is not obvious. The motion-dependent aerodynamic terms are periodic functions of the azimuth angle, which introduce shifts in the argument of the Laplace variable.

A general solution to this problem is pursued in this paper. The transfer functions between the dependent variables and the perturbations, such as those due to blade vortex interaction (BVI) effects, can be obtained explicitly. The accuracy of the proposed scheme is demonstrated by comparing results with a time-domain numerical solution of Mathieu's equation (second-order linear differential equation with periodic coefficients).

2. AEROELASTIC EQUATIONS IN THE LAPLACE DOMAIN

The aeroelastic equations governing the small departures from an equilibrium position for a rotating beam undergoing flatwise bending and torsional vibration were derived in a previous paper [1]. The following set of $2n$ second-order differential equations in the blade azimuth angle, with periodic coefficients, was obtained:

$$\mathcal{M}\ddot{x} + \mathcal{C}(\psi)\dot{x} + \mathcal{K}(\psi)x = \mathcal{F}(\psi) \qquad (1)$$

In (1), the vector of dependent variables collects the flatwise-bending slope and torsion displacement evaluated at n stations along the beam:

$$x = \{\varphi, \theta\} \qquad (2)$$

The matrix coefficients on the left-hand side are defined next:

$$\mathcal{M} = vD(M + \frac{\lambda}{2}\bar{I}_b Q_2)$$

$$\mathcal{C}(\psi) = vD\frac{\gamma}{2}\bar{I}_b(Q_1 + Q_{1s}\sin\psi) \qquad (3)$$

$$\mathcal{K}(\psi) = I + vD[Z + \frac{\gamma}{2}\bar{I}_b(Q_0 +$$

$$Q_{0s}\sin\psi + Q_{01c}\cos\psi + Q_{02c}\cos 2\psi)]$$

The vector on right-hand side represents general external loads not only generated by the blade control input but also

by aerodynamic disturbances such as BVI. For the sake of completeness, the matrices appearing on the right-hand side of (3) are listed in Appendix A.

It is important to stress that although the integrating matrix method was used here to derive the above equations, the procedure pursued in the present work is applicable to systems of linear differential equations with periodic coefficients in general. The integrating matrix technique provides a semi-analytical method of integrating the differential equations in the spatial independent variable [2]. It is particularly attractive if used as a substitute for the modal superposition technique in linear two-point boundary value problems in Aeroelasticity since no subspace truncations become necessary and the physical degrees of freedom are kept throughout the calculations.

2.1. A Laplace-domain Solution for the Hover Condition

In (3), it is important to note that when the advance ratio equals zero (helicopter flight hover condition), the terms involving products between harmonic functions of the azimuth angle reduce to zero. Hence, (1) becomes a set of linear, time-invariant differential equations. The solution of this problem in the Laplace domain yields:

$$X(\bar{s}) = \Phi_0(\bar{s})F(\bar{s}) \qquad (4)$$

where the transfer function,

$$\Phi_0(\bar{s}) = [I + DG_0(\bar{s})]^{-1} \qquad (5)$$

may be identified as the forward transmission of the system, where

$$G_0(\bar{s}) = vM\bar{s}^2 + vZ + Q(\bar{s}; \mu = 0) \qquad (6)$$

The solution of the problem closely resembles that of a fixed-wing aircraft. However, the Laplace transformation of the motion-dependent aerodynamic loads, shown in the last term of (6), involves an extension of the lift deficiency function for rotary wings onto the complex Laplace plane [3].

2.2. Laplace-domain Solution for the Forward-Flight Condition

When the forward-flight condition is analyzed, the presence of the periodic terms in (1) leads to extra difficulties. The sine and cosine harmonics of the azimuth angle appearing in (3) may be replaced by their complex counterparts:

$$\sin \ell \psi = \left(e^{i\ell\psi} - e^{-i\ell\psi}\right)/2i$$
$$\cos \ell \psi = \left(e^{i\ell\psi} + e^{-i\ell\psi}\right)/2 \qquad (7)$$

Using the shift property of Laplace transforms, which is valid for a complex α,

$$\mathcal{L}\left\{e^{-\alpha\psi}x(\psi)\right\} = X(\bar{s} + \alpha) \qquad (8)$$

the following result is obtained for the Laplace transform of (1):

$$X(\bar{s}) + D\sum_{j=-2}^{2} G_j(\bar{s})X(\bar{s} + ji) = F(\bar{s}) \qquad (9)$$

In (9), the summation is carried over two harmonics, $-2 \le j \le 2$ for any aerodynamic model for which the motion-dependent components involve the square of the local airflow velocity [4]:

$$U/\Omega R = r/R + \mu \sin \psi \qquad (10)$$

Technical difficulty arises when trying to solve (9) for $X(\bar{s})$ since this solution also involves the four additional unknowns $X(\bar{s} + ji)$. This problem has a closed mathematical solution if one recognizes that (9) may be repeated N times, each time replacing the argument $\bar{s}$ by $\bar{s} + ji$, where $-N \le j \le N$. The procedure accounts for the "missing" information related to the harmonics of the dependent variables. The method produces the exact solution as N approaches infinity. However, it was observed that very good approximations for the time intervals typical of both the low-frequency vibration and the BVI phenomenon are obtained if only a small number of harmonics is taken into consideration. The solution, then, yields a simple N-dimensional extension of the "hover" solution discussed in the previous section:

$$\mathbb{X}(\bar{s}) = \Phi(\bar{s})\mathbb{F}(\bar{s}) \qquad (11)$$

where

$$\Phi(\bar{s}) = \left[I + \begin{bmatrix} D & & \\ & \ddots & \\ & & D \end{bmatrix} \mathbb{G}(\bar{s}) \right]^{-1} \qquad (12)$$

which can also be written in a compact form:

$$\Phi_{mn}(\bar{s}) = \left[\delta_{k\ell}I + D\mathbb{G}_{k\ell}(\bar{s})\right]^{-1}$$
$$(k,\ell,m,n = 0, \pm 1, \ldots, \pm N, \ldots, \pm\infty) \qquad (12a)$$

and

$$\mathbb{X}(\bar{s}) = \left\{ \begin{array}{c} \vdots \\ X(\bar{s}+2i) \\ X(\bar{s}+i) \\ X(\bar{s}) \\ X(\bar{s}-i) \\ X(\bar{s}-2i) \\ \vdots \end{array} \right\}; \quad \mathbb{F}(\bar{s}) = \left\{ \begin{array}{c} \vdots \\ F(\bar{s}+2i) \\ F(\bar{s}+i) \\ F(\bar{s}) \\ F(\bar{s}-i) \\ F(\bar{s}-2i) \\ \vdots \end{array} \right\} \qquad (13\text{-}14)$$

$\mathbb{G}(s)$ is a matrix of band five (shown in Appendix B in the expanded form) whose elements are themselves matrix transfer functions of dimension $2n$. Hence,

$$\mathbb{G}_{k\ell}(\bar{s}) = \begin{cases} G_{k-\ell}(\bar{s} - ki) & \text{if } |k-\ell| \le 2 \\ 0 & \text{if } |k-\ell| > 2 \end{cases}$$
$$(k,\ell = 0, \pm 1, \ldots, \pm N, \ldots, \pm\infty) \qquad (15)$$

where

$$G_0(\bar{s}) = v\bar{s}^2 M + vZ +$$
$$\frac{v\gamma}{2}\bar{I}_b[\bar{s}^2 Q_2 + \bar{s}Q_1(\bar{s}) + Q_0(\bar{s})]$$
$$G_{\pm 1}(\bar{s}) = \frac{v\gamma}{4}\bar{I}_b[-(\mp i\bar{s} + 1)Q_{1s}(\bar{s}) \pm iQ_{0s}(\bar{s}) + Q_{01c}] \qquad (16)$$
$$G_{\pm 2}(\bar{s}) = \frac{v\gamma}{4}Q_{02s}(\bar{s})$$

It is worthwhile to point out that in hover $\mathbb{G}(\bar{s})$ collapses to the element $G_0(\bar{s})$ alone. Therefore, the latter represents only a particular case of a more general transfer function associated with the forward transmission of the system.

The general solution implied by (11) is redundant because it involves integer shifts of $X(\bar{s})$ along the imaginary axis. Therefore, it suffices to consider the central block of $\mathbb{X}(\bar{s})$. An Nth-order approximation to the exact solution of the problem then yields:

$$X(\bar{s}) = \Phi_{0\ell}(\bar{s})\mathbb{F}(\bar{s}) \quad (\ell = 0, \pm 1, \ldots, \pm N) \qquad (17)$$

3. VALIDATION OF THE METHOD: A SOLUTION TO MATHIEU'S EQUATION

In order to validate the proposed method, the following Mathieu's equation was solved:

$$\ddot{x} + (1 + \mu \sin t)x = f(t) \qquad (18)$$

The coefficient of the periodic term was set equal to one to evaluate a possible critical case regarding convergence. The mathematical problem resembles one of a helicopter blade in forward flight condition with advance ratio one, except for the absence of the higher harmonics. The Laplace transform of (18) then yields:

$$(1+s^2)X(s)+\tfrac{1}{2i}X(s-i)-\tfrac{1}{2i}X(s+i)=F(s) \qquad (19)$$

where the initial conditions were moved to the right-hand side. Using the proposed scheme, (19) was repeated an infinite number of times, each time shifting the argument of the Laplace transform by $\pm i$, yielding:

$$A_{k\ell}X_\ell = F_\ell \qquad (k,\ell=0,\pm 1,\dots,\pm N,\dots,\pm\infty) \qquad (20)$$

where A is a matrix of band size three:

$$A_{k\ell}=[1+(s+ki)^2]\delta_{k\ell}$$
$$+\begin{cases} \tfrac{1}{2i}(\ell-k) & \text{if} \quad |k-\ell|\le 1 \\ 0 & \text{if} \quad |k-\ell|>1 \end{cases} \qquad (21)$$

and the augmented dependent variable and right-hand side vectors are, respectively:

$$X_\ell = X(s+\ell i)$$
$$F_\ell = F(s+\ell i) \qquad (22)$$

The solution of this problem may be obtained using Cramer's rule. Since one is only interested in the central element of X, a single ratio of two determinants produces the desired solution:

$$X_0 = X(s) = \left|\tilde{A}\right|/|A| \qquad (23)$$

where the matrix shown in the numerator of (23) is generated by replacing the central column of A by F:

$$\tilde{A}_{k\ell}=\begin{cases} A_{k\ell} & \text{if} \quad \ell\ne 0 \\ F_k & \text{if} \quad \ell=0 \end{cases} \qquad (24)$$

The solution in terms of the original independent variable is obtained taking the inverse Laplace transform of (23). As an illustration, this is done for $F(s)=s$ (system response to a unitary initial displacement) in Appendix C. In Figure 1, the first five approximations for the solution are compared with the result obtained by direct numerical integration of (18). One can observe that a very accurate approximation is achieved with N=4.
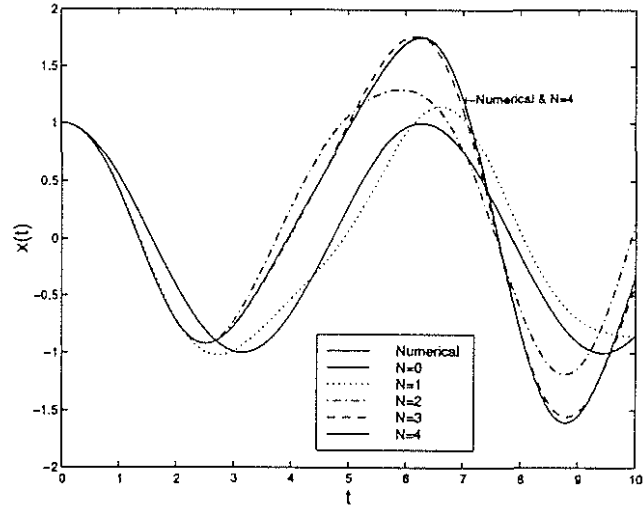
Figure 1 Successive approximations for the solution of Mathieu's equation using the proposed Laplace transform method. Initial conditions $x(0)=1$; $\dot{x}(0)=0$ are assumed ($\mu=1$).

4. RESULTS FOR A TYPICAL ROTOR BLADE

A series of numerical examples based on a typical reduced-scale four-blade rotor (Tables 1 and 2) are shown to illustrate the technique. The lift deficiency function at local stations along the blade was approximated in the frequency domain by the ratio of third-order polynomials:

$$C(\bar{s})=\frac{0.5\bar{s}^3+0.69\bar{s}^2+0.2274\bar{s}+0.0151}{\bar{s}^3+1.133\bar{s}^2+0.2852\bar{s}+0.01503} \qquad (25)$$

where the argument of C was based on the local mean average air velocity:

$$\bar{s}=sb/\Omega r=\bar{s}b/r \qquad (26)$$

The proposed method allows the computation of the bode diagrams associated with localized displacements along the blade due to a Dirac-delta function input. This example is important because it produces the transfer function between a distributed aerodynamic perturbation applied along the blade and a selected dependent variable. Moreover, the example simulates the effect of a parallel blade vortex interaction (BVI) occurring in the forward-flight condition. Hence,

$$F(\bar{s})=1 \qquad (27)$$

at all $n=9$ stations taken along the blade.

Table 1 Typical Blade Dynamics ($\Omega = 110 \text{ rad} / s$)

modal frequencies below 30/rev (n=9) (1/rev)	modal description	
	bending mode number	torsion mode number
1.105	1	-
2.749	2	-
3.523	-	1
4.484	3	-
7.484	4	-
9.938	5	-
10.16	-	2
13.35	6	-
17.09	-	3
23.89	7	-

Table 2 Typical Blade Parameters

parameter	value
a	-0.1
$\bar{b} = b/R$	0.0302
$\bar{I}_b = I_b/mR^3$	0.0334
$\gamma = 4\pi\rho bR^4/I_b$	5.215
$\nu = m\Omega^2 R^4/EI_{ref}$	81.29

4.1 Convergence Studies

In the following examples, the blade advance ratio is assumed to be 0.15. In Figures 2 and 3, one can observe that convergence was already achieved with N=2 for a range of frequencies up to 30/rev (there is no practical distinction between the curves for N=2 and N=3). One can also observe that for this relatively low advance ratio, the frequency response is dominated by the natural modes of the spinning blade, which are captured by the time-invariant model (N=0) as well. However, the latter approximation is particularly poor for frequencies in the neighborhood of 8/rev, which are considered to be critical for vibration control in a four-blade helicopter rotor. Obviously, the time-varying behavior of the system is expected to become more pronounced as the forward speed increases.
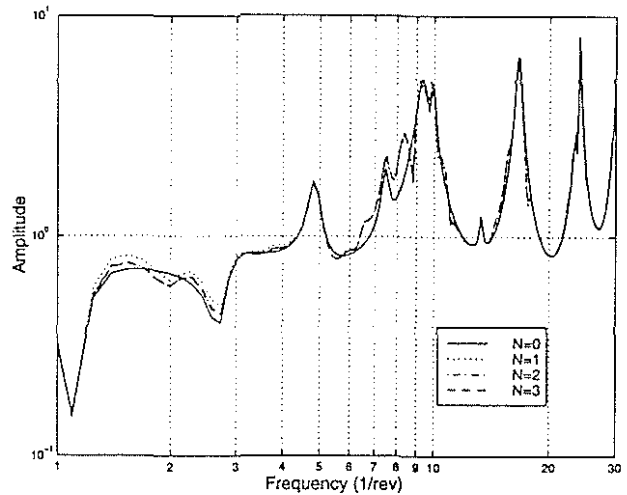
Figure 2 Amplitude of the transfer function between the torsional displacement at the tip and a sudden uniform pressure perturbation applied along a rotor blade in forward flight. Convergence study assuming advance ratio 0.15.
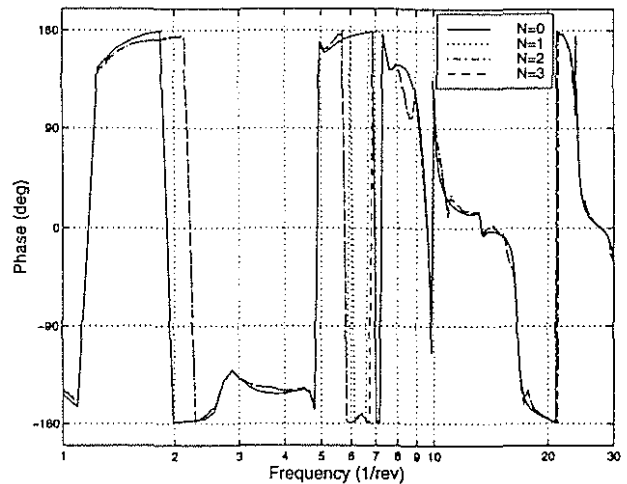
Figure 3 Phase of the transfer function between the torsional displacement at the tip and a sudden uniform pressure perturbation applied along a rotor blade in forward flight. Convergence study assuming advance ratio 0.15.

4.2 Effect of Advance Ratio

As the advance ratio increases, the solution behavior departs more significantly from the time-invariant. In Figures 4 and 5, respectively the magnitude and phase of the frequency response associated with the torsional displacement computed at the tip of the blade is analyzed for the advance ratios 0, 0.15 and 0.30. It is worthwhile to

point out that the model captures a well-known behavior of rotor blades in forward flight: vibration is expected to increase with the rotor forward speed. Especially at frequencies between 2 and 3, and between 5 and 8/rev, the transfer function shows an increase in amplitude, reflecting the interaction between the first and second torsional natural modes of the spinning blade and the harmonic terms characteristic of the blade aerodynamics in the forward fight condition.
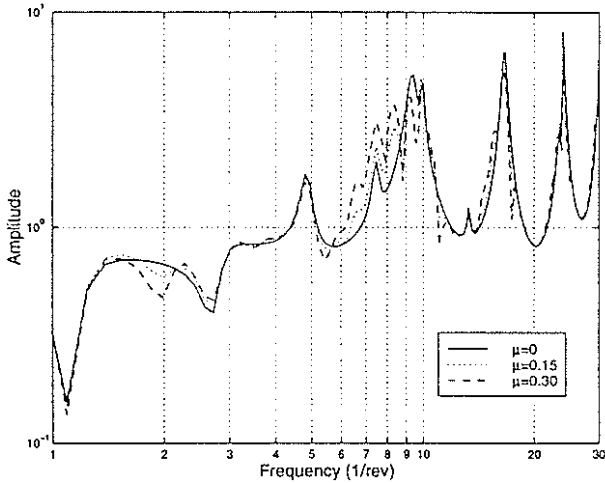
Figure 4 Amplitude of the transfer function between the torsional displacement at the tip and a sudden uniform pressure perturbation applied along a rotor blade in forward flight. Advance ratio effect (N=3 for the time-varying cases).
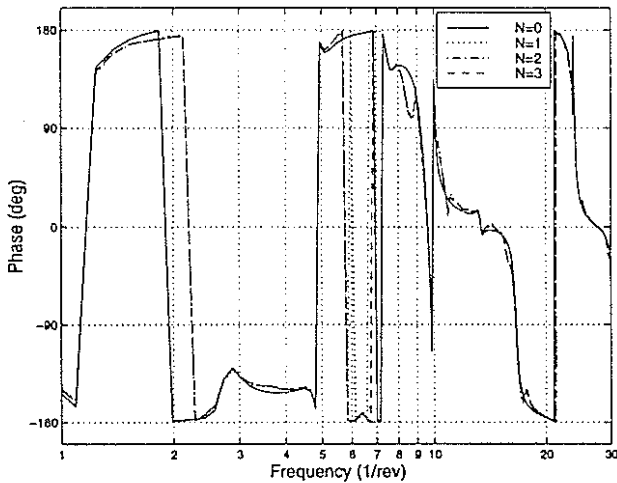
Figure 5 Phase of the transfer function between the torsional displacement at the tip and a sudden uniform pressure perturbation applied along a rotor blade in forward flight. Advance ratio effect (N=3 for the time-varying cases).

4.3. Radial Distribution

The magnitude of the transfer functions associated with the advance ratio 0.15 are plotted next for the stations $r/R=1$, 0.778, 0.556 and 0.344, respectively. Figure 6 depicts the bending displacement and Figure 7 the corresponding torsional displacement at the same stations. These figures, suggest that the amplitude of the transfer functions are, as in a fixed wing case, very much related to the natural mode shapes of the spinning blade.
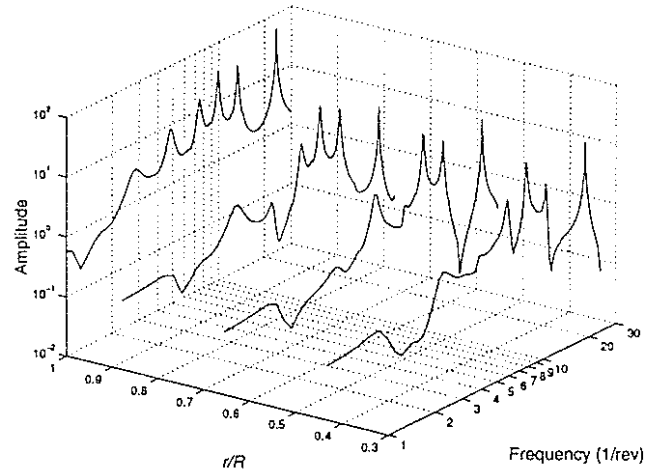
Figure 6 Amplitude of the transfer functions between the bending displacement at different stations and a uniform pressure perturbation applied along a rotor blade in forward flight (μ=0.15).
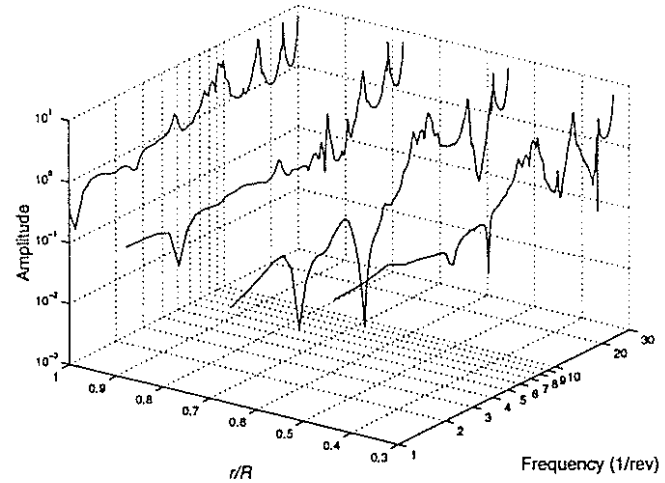
Figure 7 Amplitude of the transfer functions between the torsional displacement at different stations and a uniform pressure perturbation applied along a rotor blade in forward flight (μ=0.15).

5. CONCLUSIONS

In the paper, a method based on Laplace transformation to solve the aeroelastic problem of a rotor blade in forward flight was presented. The method can be used to transform a system consisting of a set of linear differential equations carrying periodic coefficients into an approximate equivalent time-invariant in general. First, a distinct form of Mathieu's equation was solved to investigate the convergence of the method for the time intervals useful to helicopter individual blade control applications. Second, the two-degree-of-freedom (flatwise bending and torsion) aeroelastic equations of a typical helicopter blade in forward flight were solved to demonstrate the method. In particular, the continuous frequency-domain transfer functions from a sudden pressure distribution applied along the blade to localized displacements at selected stations were obtained. The solution resembled one of a fixed wing, with the natural modes of the spinning blade dominating the frequency response spectrum. However, as the advance ratio increased, significant contributions from the original time-varying terms were observed, indicating that the latter effect must not be neglected when synthesizing non-harmonic individual blade control laws. In particular, the transfer functions demonstrate that at some critical harmonic frequencies of the blade passage, an increase in the dynamic response of the blade is already observed at moderate advance ratios. The latter effect becomes more pronounced as the forward speed increases.

REFERENCES

1. Nitzsche, F., "A New Individual Blade Control Approach to Attenuate Rotor Vibration," Paper No. 8, *Proceedings:* 22nd European Rotorcraft Forum, Vol. I, Brighton, UK, September 17-19, 1996.

2. Lehman, L. L., "Hybrid State Vector Methods for Structural Dynamic and Aeroelastic Boundary Value Problems," NASA CR-3591, 1982.

3. Friedmann, P. P., "Arbitrary Motion Unsteady Aerodynamics and its Application to Rotary-Wing Aeroelasticity," *Journal of Fluids and Structures*, Vol. 1, 1987, pp. 71-93.

4. Isaacs, R., "Airfoil Theory for Flows of Variable Velocity," *Journal of the Aeronautical Sciences*, Vol. 12, No. 1, 1945, pp. 113-117.

5. Myrtle, T. F. and Friedmann, P. P., "Unsteady Compressible Aerodynamics of a Flapped Airfoil with Applications to Helicopter Vibration Reduction," Paper AIAA-97-1083, *38th AIAA/ASME/ASCE/AHS/ASC Structures, Structural Dynamics and Materials Conference and Exhibit*, Washington, DC, Part 1, pp. 224-240.

6. Vepa, R., "Finite-State Modeling of Aeroelastic Systems," NASA CR-2779, 1977.

7. Karpel, M., "Design for Active Flutter Suppression and Gust Alleviation Using State-Space Aeroelastic Modeling," *Journal of Aircraft*, Vol. 19, No. 3, 1982, pp. 221-227.

8. Johnson, W., *Helicopter Theory*, Princeton University Press, 1980, pp.492-498.

9. McLachlan, N. W., *Theory and Applications of Mathieu Functions*, Oxford University Press, New York, 1947.

APPENDIX A: COEFFICIENT MATRICES

In (A1), matrices of structural influence coefficients that appear in the main text are defined. The non-dimensional quantities are obtained using the following normalization: $\bar{d}_{ij} = d_{ij}R/EI_{ref}$, $\bar{m} = m/m_{ref}$, $\bar{T} = T/\Omega^2 R^2 m_{ref}$ and $\bar{r}_\theta = r_\theta/R$.

$$D = \begin{bmatrix} J[\bar{d}_{11}]J_1 & J[\bar{d}_{13}]J_1 \\ J[\bar{d}_{13}]J_1 & J[\bar{d}_{33}]J_1 \end{bmatrix}$$

$$M = \begin{bmatrix} J_1[\bar{m}]J & 0 \\ 0 & [\bar{m}\bar{r}_\theta^2] \end{bmatrix} \qquad (A1)$$

$$Z = \begin{bmatrix} [\bar{T}] & 0 \\ 0 & [\bar{m}\bar{r}_\theta^2] \end{bmatrix}$$

In (A2), the aerodynamic influence coefficient matrices are defined. Only those with non-zero circulatory components are dependent on the Laplace variable:

$$Q_2 = \tfrac{1}{2}J_2 Q_2^{NC} J_3$$

$$Q_1(\bar{s}) = J_2\big(\mathbb{C}(\bar{s})Q_1^Q + \tfrac{1}{2}Q_1^{NC}\big)['\{\bar{r},\bar{r}\}]J_3$$

$$Q_0(\bar{s}) = J_2\mathbb{C}(\bar{s})Q_0^Q\big(['\{\bar{r},\bar{r}\}]^2 + \tfrac{1}{2}['\{\mu,\mu\}]^2\big)J_3$$

$$Q_{1s}(\bar{s}) = J_2\big(\mathbb{C}(\bar{s})Q_1^Q + \tfrac{1}{2}Q_1^{NC}\big)['\{\mu,\mu\}]J_3 \qquad (A2)$$

$$Q_{0s}(\bar{s}) = 2J_2\mathbb{C}(\bar{s})Q_0^Q['\{\mu,\mu\}]['\{\bar{r},\bar{r}\}]J_3$$

$$Q_{02c}(\bar{s}) = -\tfrac{1}{2}J_2\mathbb{C}(\bar{s})Q_0^Q['\{\mu,\mu\}]^2 J_3$$

$$Q_{01c} = \tfrac{1}{2}J_2 Q_0^{NC}['\{\mu,\mu\}]J_3$$

where $\bar{r} = r/R$. The next, are constant matrices, dependent both on the flight condition and the blade local geometric properties:

$$Q_2^{NC} = \begin{bmatrix} [\bar{b}] & ['a\bar{b}^2] \\ -['a\bar{b}^2] & -['(\tfrac{1}{8}+a^2)\bar{b}^3] \end{bmatrix}$$

$$Q_1^{NC} = \begin{bmatrix} 0 & -[\bar{b}] \\ 0 & -['(\tfrac{1}{2}-a)\bar{b}^2] \end{bmatrix}$$

$$Q_0^{NC} = \begin{bmatrix} 0 & -[\bar{b}] \\ 0 & [\bar{b}^2] \end{bmatrix}$$

(A3)

$$Q_1^Q = \begin{bmatrix} I & -['(\tfrac{1}{2}-a)\bar{b}] \\ -['(\tfrac{1}{2}+a)\bar{b}] & ['(\tfrac{1}{4}-a^2)\bar{b}^2] \end{bmatrix}$$

$$Q_0^Q = \begin{bmatrix} 0 & -I \\ 0 & ['(\tfrac{1}{2}+a)\bar{b}] \end{bmatrix}$$

Finally,

$$J_1 = (B_1 - I)J$$

$$J_2 = \begin{bmatrix} J_1 & 0 \\ 0 & -I \end{bmatrix}$$

$$J_3 = \begin{bmatrix} J & 0 \\ 0 & I \end{bmatrix}$$

(A4)

are integrating matrix operators. A matrix collecting the section lift deficiency coefficients is also defined in (A2):

$$\mathbb{C}(\bar{s}) = ['\{C(\bar{s}), C(\bar{s})\}]$$

(A5)

The components of this matrix may be derived using techniques that are usually based on rational function approximations (Padé approximants) of aerodynamic loads obtained from oscillatory time-response data [5]. This is an extension of methods generally used for fixed wing aircraft [6, 7]. In the present work, the lift deficiency coefficients were based on Greenberg's theory with the reduced frequency based on the mean local velocity [8]. The latter is an acceptable approximation for low advance ratios and stations of the blade not very close to the hub.

APPENDIX B: MATRIX $\mathbb{G}(s)$

$\mathbb{G}(\bar{s}) =$

$$\begin{bmatrix} \ddots & \ddots & \ddots & \ddots & \ddots \\ G_2(\bar{s}+2i) & G_1(\bar{s}+2i) & G_0(\bar{s}+2i) & G_{-1}(\bar{s}+2i) & G_{-2}(\bar{s}+2i) & 0 & \cdots \\ 0 & G_2(\bar{s}+i) & G_1(\bar{s}+i) & G_0(\bar{s}+i) & G_{-1}(\bar{s}+i) & G_{-2}(\bar{s}+i) & 0 & \cdots \\ \cdots & 0 & G_2(\bar{s}) & G_1(\bar{s}) & G_0(\bar{s}) & G_{-1}(\bar{s}) & G_{-2}(\bar{s}) & 0 & \cdots \\ \cdots & 0 & G_2(\bar{s}-i) & G_1(\bar{s}-i) & G_0(\bar{s}-i) & G_{-1}(\bar{s}-i) & G_{-2}(\bar{s}-i) & 0 \\ \cdots & 0 & G_2(\bar{s}-2i) & G_1(\bar{s}-2i) & G_0(\bar{s}-2i) & G_{-1}(\bar{s}-2i) & G_{-2}(\bar{s}-2i) \\ & & \ddots & \ddots & \ddots & \ddots & \ddots \end{bmatrix}$$

(B1)

APPENDIX C: SOLUTION OF MATHIEU'S EQUATION BY LAPLACE TRANSFORM

Consider the response of (18) to the initial condition $x(0) = 1$. The solution is given by the ratio of the infinite determinants described in (23):

$$X(s) = \left. \begin{array}{|ccccccccc|}
\ddots & \ddots & 0 & \vdots & \vdots & \vdots & \vdots & \vdots & \vdots \\
\ddots & 1+(s+3i)^2 & 1/2i & 0 & s+3i & 0 & 0 & 0 & \cdots \\
0 & -1/2i & 1+(s+2i)^2 & 1/2i & s+2i & 0 & 0 & 0 & \cdots \\
\cdots & 0 & -1/2i & 1+(s+i)^2 & s+i & 0 & 0 & 0 & \cdots \\
\cdots & 0 & 0 & -1/2i & s & 1/2i & 0 & 0 & \cdots \\
\cdots & 0 & 0 & 0 & s-i & 1+(s-i)^2 & 1/2i & 0 & \cdots \\
\cdots & 0 & 0 & 0 & s-2i & -1/2i & 1+(s-2i)^2 & 1/2i & 0 \\
\cdots & 0 & 0 & 0 & s-3i & 0 & -1/2i & 1+(s-3i)^2 & \ddots \\
\vdots & \vdots & \vdots & \vdots & \vdots & \vdots & 0 & \ddots & \ddots \\
\hline
\ddots & \ddots & 0 & \vdots & \vdots & \vdots & \vdots & \vdots & \vdots \\
\ddots & 1+(s+3i)^2 & 1/2i & 0 & 0 & 0 & 0 & 0 & \cdots \\
0 & -1/2i & 1+(s+2i)^2 & 1/2i & 0 & 0 & 0 & 0 & \cdots \\
\cdots & 0 & -1/2i & 1+(s+i)^2 & 1/2i & 0 & 0 & 0 & \cdots \\
\cdots & 0 & 0 & -1/2i & 1+s^2 & 1/2i & 0 & 0 & \cdots \\
\cdots & 0 & 0 & 0 & -1/2i & 1+(s-i)^2 & 1/2i & 0 & \cdots \\
\cdots & 0 & 0 & 0 & 0 & -1/2i & 1+(s-2i)^2 & 1/2i & 0 \\
\cdots & 0 & 0 & 0 & 0 & 0 & -1/2i & 1+(s-3i)^2 & \ddots \\
\vdots & \vdots & \vdots & \vdots & \vdots & \vdots & 0 & \ddots & \ddots
\end{array} \right. \tag{C1}$$

The ratios of finite determinants obtained by successively expanding the dimension from the central elements of the numerator and denominator of (C1) generate approximate solutions of increasing order: $N=0$ corresponds to a ratio of determinants of dimension 1, $N=1$ to a ratio of determinants of dimension 3, etc. The first five approximations ($N = 0, 1, \ldots, 4$) to the exact solution in the Laplace domain are given by:

$$X(s) = \left\{ \begin{array}{ll}
\dfrac{s}{s^2+1} & (N=0) \\[2ex]
\dfrac{s^5+4s^3-s^2}{s^6+5s^4+7/2\,s^2} & (N=1) \\[2ex]
\dfrac{s^9+14s^7-s^6+48s^5-10s^4+41s^3-41/4\,s^2+99/16\,s+3/4}{s^{10}+15s^8+62s^6+85s^4+595/16\,s^2-5/16} & (N=2) \\[2ex]
\dfrac{s^{13}+34s^{11}-s^{10}+783/2\,s^9-30s^8+3825/2\,s^7-543/2\,s^6+7913/2\,s^5-1701/2\,s^4+2700s^3-1421/2\,s^2+392s+46}{s^{14}+35s^{12}+851/2\,s^{10}+2300s^8+46233/8\,s^6+49485/8\,s^4+37319/16\,s^2-79/4} & (N=3) \\[2ex]
\dfrac{\begin{array}{c}s^{17}+68s^{15}-s^{14}+1772s^{13}-64s^{12}+22902s^{11}-1516s^{10}+251971 7/16\,s^9-16862s^8-4546955/8\,s^7-364019/4\,s^6+980861s^5-43047 1/2\,s^4+\ldots \\ 9916053/16\,s^3-10089417/64\,s^2+22397701/256\,s+659583/64\end{array}}{s^{18}+69s^{16}+1840s^{14}+24670s^{12}+2882533/16\,s^{10}+11543003/16\,s^8+12097955/8\,s^6+23476953/16\,s^4+133608341/256\,s^2-1132835/256} & (N=4) \\[2ex]
\vdots &
\end{array} \right. \tag{C2}$$

The general form for the inverse Laplace transform of (C2) was found to be a superposition of a convergent and divergent series (as $t \to \infty$). The overall nature of the solution depends on the relative magnitude of the corresponding coefficients of the sine and cosine terms:

$$x(t) = \sum_{i=0}^{N+1} [e^{k_i t}(a_i \cos \omega_i t + b_i \sin \omega_i t) + e^{-k_i t}(c_i \cos \omega_i t + d_i \sin \omega_i t)] \tag{C3}$$

The arguments k_i and ω_i of the series expansion are respectively the real and imaginary parts of the poles of $X(s)$, and the associated coefficients are obtained from the corresponding residues. These parameters are listed in Table C1 for the first five approximations.

Table C1 Coefficients of Mathieu's Equation Series Solution (Inverse Laplace Transform)

N	$\omega_0, \omega_1, \ldots \omega_{N+1}$	$k_0, k_1, \ldots k_{N+1}$	$a_0, a_1, \ldots a_{N+1}$	$b_0, b_1, \ldots b_{N+1}$	$c_0, c_1, \ldots c_{N+1}$	$d_0, d_1, \ldots d_{N+1}$
0	0	0	0	0	0	0
	1	0	1	0	0	0
1	0	0	0	0	0	0
	0.9174	0	9.5297×10^{-1}	-3.2865×10^{-1}	0	0
	2.0392	0	4.7732×10^{-2}	1.479×10^{-1}	0	0
2	0	9.0813×10^{-2}	1.7939×10^{-1}	0	-1.0252×10^{-2}	0
	1.0253	6.9533×10^{-2}	6.3500×10^{-1}	-3.3499×10^{-1}	1.4237×10^{-1}	-4.6264×10^{-2}
	1.9180	0	6.2499×10^{-2}	1.7237×10^{-1}	0	0
	3.0392	0	-8.9933×10^{-3}	2.8920×10^{-3}	0	0
3	0	9.1017×10^{-2}	1.7543×10^{-1}	0	-5.2232×10^{-3}	0
	1.0003	9.0916×10^{-2}	7.4603×10^{-1}	-3.7305×10^{-1}	2.6642×10^{-2}	3.0449×10^{-2}
	2.0253	6.9534×10^{-2}	6.3509×10^{-2}	9.7540×10^{-2}	5.2091×10^{-3}	2.3832×10^{-2}
	2.9180	0	-1.1496×10^{-2}	4.1679×10^{-3}	0	0
	4.0392	0	-9.4480×10^{-5}	-2.9381×10^{-4}	0	0
4	0	9.1017×10^{-2}	1.7512×10^{-1}	0	-5.5134×10^{-3}	0
	1.0000	9.1017×10^{-2}	7.4351×10^{-1}	-3.5297×10^{-1}	2.2537×10^{-2}	1.1342×10^{-2}
	2.0003	9.0916×10^{-2}	7.7358×10^{-2}	1.1640×10^{-1}	-5.6096×10^{-3}	3.8084×10^{-3}
	3.0253	6.9534×10^{-2}	-5.7802×10^{-3}	4.2049×10^{-3}	-1.4781×10^{-3}	2.4374×10^{-4}
	3.9180	0	-1.4532×10^{-4}	-4.0082×10^{-4}	0	0
	5.0392	0	6.0240×10^{-6}	-1.9371×10^{-6}	0	0

From Table C1 one can observe how the series converge to the exact solution. As the order of system increases, the frequencies associated with the lower harmonics approach the corresponding integer numbers. At the same time, the magnitude of the coefficients associated with the higher harmonics becomes increasing smaller.

Another interesting observation inferred by inspection of Table C1 is that as the order increases and new poles are added to the characteristic equation, the newly found roots first appear as pure complex conjugate pairs, whereas the previously obtained roots split into two complex conjugate pairs. The latter pairs have non-zero real parts with mirror images about the imaginary axis.

The solution to this problem can be expressed in terms of Mathieu's function [9]. However, in the present study, direct numerical integration of the equation using a 5th order Runge-Kutta method is employed. A plot comparing the inverse Laplace transform solution with the numerical integration is shown in the main text.